Geomorphology 301 (2018) 1–9

Contents lists available at ScienceDirect

Geomorphology

journal homepage: www.elsevier.com/locate/geomorph

A new approach to triggering mechanism of volcano landslides based on zeta potential and surface free energy balance

I. Plaza [a], A. Ontiveros-Ortega [a,b,*], J. Calero [c], C. Romero [d]

[a] Department of Physics, University of Jaén, A-3, 23071 Jaén, Spain
[b] Andalusian Institute of Geophysics, University of Granada, 18071 Granada, Spain
[c] Department of Geology, University of Jaén, B-3, 23071 Jaén, Spain
[d] Department of Geography, University of La Laguna, Spain

ARTICLE INFO

Article history:
Received 6 April 2017
Received in revised form 5 October 2017
Accepted 12 October 2017
Available online 2 November 2017

Keywords:
Almagre
Zeta potential
Surface free energy
Volcanic ash
Landside

ABSTRACT

The layers of Almagre (iron-rich deposits) from Tenerife Island are the result of thermal metamorphism of soils in contact with lava flow (1073–1273 K). These layers of small thickness relative to the basaltic wash, are interesting for geotechnical study, because the stability of the deposits is determined by the weakest element, in this case Almagre, which acts as a sliding plane. The flow of maritime air over the hillsides of the volcanic islands increases the content of cations in ashes deposits. This modifies the superficial properties of material that composes the substratum. This modification affects the retention of water and the cohesion of material making up the deposit. The results show that the presence of sodium and magnesium increased the hydrophobicity of the material, which had a weak water retention capacity and strong cohesion at basic pH. When there is iron in solution, repulsion between the particles is greater than one obtained with other studied electrolytes. Hence, the deposit is less stable, and Almagre under saturated water conditions constitutes an ideal layer for landslides.

1. Introduction

Large volcanic landslides are a common phenomenon in the Canary Islands; >20 huge volcanic landslides were detected during the last decades around this archipelago (Hürlimann et al., 2004). Recent studies show that there are two main causes of these landslides: structural axes and residual soils.

The objective of this work is to improve the insights into the causes of large volcanic landslides focusing mainly on the existence of these residual soils.

The Island of Tenerife in the Canary Islands of Spain (Fig. 1) has been studied by the international scientific community. This is indicated by a multitude of articles published in recent years related to the consequences of a potential slide of hillsides (e.g., tsunami, loss of life, economic losses (Broothaerts et al., 2012; BASU and DE, 2003). These studies analyzed the topography, extent of present vegetation, and geotechnical parameters of the area (Crozier and Glade, 2005), and calculated hillside safety factors via simulations (Zhou et al., 2003) based on different models of the area.

Our study is based on the layer of eruptive material known as "Almagre," selected for its unique geologic history (Ancochea et al., 1990–1999) and characteristic geotechnical contacts with the low and top layers. This materials consists of layers (a few millimeters to meters in thickness) of iron oxides, either magnetite (Fe_3O_4) or hematite (Fe_2O_3), alternating with bands (iron-poor) of eruptive materials (Katsuta et al., 2012). As to its origin, there is no clear consensus (Perkins, 2009). Several models have been proposed to explain its genesis: deposition in environmental lacustrine, hydrothermal, evaporite, meteorization … which assumes the planes of typical slides in Tenerife (Martí, 1997; Hürlimann et al., 2004)". The Almagres is widespread residual soils, which were detected at many sites in the Tenerife. Studies on residual soils showed that their geotechnical properties depend on many factors including the type of parent rock, climate, time, etc., and strongly differ from sedimentary soils (Blight, 1997). The stratigraphic data indicate that residual soils above ash fall deposits have a very limited extent and those formed on lava flows have only a very small thickness. In contrast, the soils formed on phonolitic pyroclastic deposits have generally a wide extent and a thickness of several decimeters. Weathering processes changed such pyroclastic deposits, produced by explosive eruptions of phonolitic magmas, into residual soils characterized by their red color. Later the residual soil was covered by a lava flow, further modifying the soil by thermal processes. Thus, the residual soils are characterized by their double cementation: firstly by the lithification processes during the deposition of the hot pyroclastic material and secondly by the thermal alteration from the lava flow covering the soil layer (Hürlimann et al., 2004).We characterize interfacial properties of Almagre and their modification in association with the presence of various electrolytes (Na-Mg-Fe) and different pH values.

* Corresponding author at: Department of Physics, University of Jaén (Spain), Campus Universitario de las Lagunillas s/n, Edificio A-3 dep.414, 23071 Jaén, Spain.
E-mail address: aontiver@ujaen.es (A. Ontiveros-Ortega).

https://doi.org/10.1016/j.geomorph.2017.10.009
0169-555X/

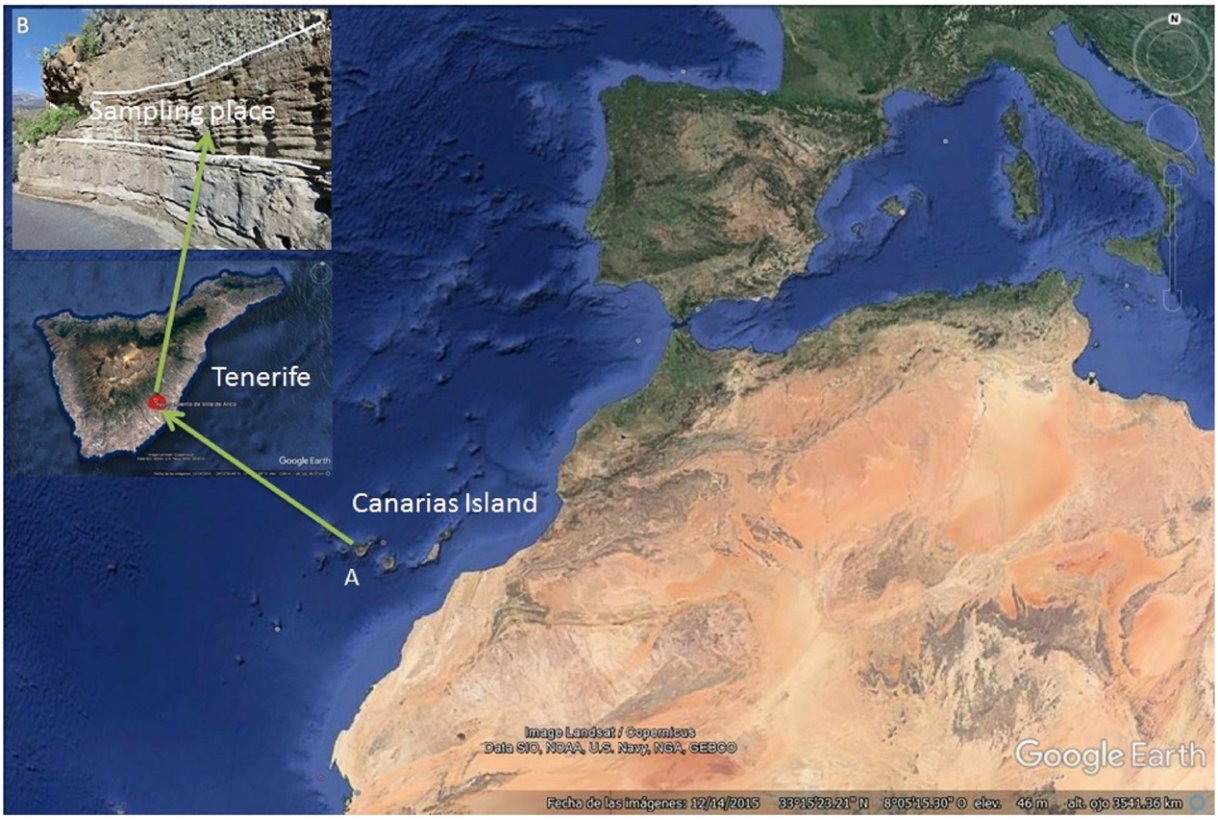

Fig. 1. Location of the island is relative to the Canary Island, and detailed presentation of the study site.

1.1. Geologic history and tectonic context of Tenerife

The geologic history of the Tenerife in Canary Islands began 12 Ma ago. It has been investigated by numerous researchers ((Carracedo et al., 2007–2011), (Longpré et al., 2009)). First it emerged I build acquaintance as "Roque de Conde" (11,6–6.4 Ma), later "Anaga" (8–3.2 Ma) and "Teno" (7.4–4.5 Ma). The geologic characteristics were investigated by Ancochea et al. (1990 & 1999), Churakov and Gimmi (2011), Martí (1997), Soto et al. (1999) and Rošic et al. (2012).

The origin of the volcanism is open to debate. We sampled in the complex called "Edificio de las Cañadas" (or Las Cañadas for short). This complex is in the southeastern part of the island, near the municipality of Guimaras. Nearby is a landslide with a volume of material >120 km^3 and an approximate age of 1 Ma. It is not the only landslide; another in Las Cañadas is dated 180,000 years ago (Masson et al., 2002).

The geologic history of Las Cañadas is marked by explosive-type volcanism, with the emission of pyroclastic clouds. Between the formation of Las Cañadas I and the II was a period of erosion and relative volcanic tranquility.

Almagre is a layer of very unique origin. It formed when materials of eroded or organic soil were buried by lava flows. These deposits are rich in iron. They are principally reddish, caused by alteration of minerals with iron, and show differential erosion in the deposit.

The above causes contact metamorphism in sedimentation of materials in previous periods and subsequent erosion, owing to layers of lava and pyroclastic expelled during this stage that buried the materials studied here. To all this must be added the effect of seawater, which in ordinary conditions contains a wide range of dissolved ions (mainly $Cl^- > Na^+ > Mg^{2+}$). Sea breezes have high moisture content, so rocks not in direct contact with seawater still experience its effects and their initial characteristics are thereby changed.

In many cases, the stratovolcanoes such as Teide Volcano, present steep slopes. Consequently they are susceptible to sudden and catastrophic failure (Bommer, 2002). Thus, earthquake-induced landslides in the Canary Islands constitute significant natural hazards. Mitigation of the landslide hazard there requires thorough understanding of the behavior of these volcanic deposits under static and dynamic conditions. The soil shows a general tendency to form aggregations of clay particles, usually showing different structures and levels of cementation. The cohesion of soils depends on several factors. Rheology properties in aqueous media are influenced by interactions between particles. The control of flocculation phenomena, adsorption, wetting, and rheological properties of dispersion depends on particle interactions (Bailey et al., 2009; Cockell, 2010; Churakov and Gimmi, 2011; Rošic et al., 2012; Kadar et al., 2014; Ontiveros-Ortega et al., 2014, 2016; Plaza et al., 2015; Baumgarten et al., 2012–2013).

Much of the scientific and technological interest in clay minerals derives from their interfacial interactions with colloidal particles (clays and other minerals) in the presence of a liquid, usually water.

Almagre layers are distributed throughout the island of Tenerife Fig. 1 (A). We chose a study area in the southwest part of the island of Tenerife (Mt. Teide), along local road TF-28. Samples were taken in a ravine in the nearby locality of Villa de Arico, see Fig. 1 (B).

2. Methods

2.1. Preparation of samples and description used materials

The samples were prepared before chemical and mineralogical analyses, they were immersed and washed by distilled water and Later they were left to dry at a temperature of 343,15 K over 48 h. Then, particles of diameter >2 mm were removed by sieving. Finally,

the samples were crushed by an agate mortar so all had a similar texture and particle size distribution.

All reagents and chemicals used were of analytical grade (Merck KGaA and Sigma-Aldrich Co. LLC, Germany). Water for surface free energy determination was twice-distilled, and Milli-Q reagent-grade water was used for electrokinetic measurements.

2.2. Chemical analysis of volcanic deposits

To characterize the samples chemically, we used fluorescence of beams-X technology. The equipment is a wavelength dispersive X-Ray fluorescence spectrometer (WDXRF) S4 EXPLORER model PIONER from Bruker AXS Inc. (Madison, Wisconsin USA). The spectrometer analyzes elements from carbon to uranium in a wide variety of samples with accuracy and precision. The source for sample excitation was an X-ray tube with rhodium anode and Be window of 75 μm. The tube and X-ray generator are designed to provide a maximum output of 4 kW with applicable maximum voltage and current 60 KV and 150 mA, respectively. There were two collimators, 0.23° and 0.46°, and five crystal analyzers, OVO-55, PET, Ge, LiF220 and LiF200. The instrument was equipped with two sensors (sealed proportional counter and scintillation counter), whose movement is controlled by a high-precision goniometer covering the entire instrumental measurement range. Samples were made into tablet form using a hydraulic press (model MIGNON SS, Nannetti, Faenza, Italy).

2.3. SEM photography

Scanning electron microscope (SEM) photography allows the definition and identification of the geometric disposition of gaseous bladders and/or volcanic glass (Holtz and Kovacs, 1981).

A SEM was used with voltage of acceleration 25 kV (S-510; Hitachi Ltd., Tokyo) and an energy-dispersive X-ray detector of (EDAX; Rontec GmbH, Berlin). Samples of ash under the only treatment were mounted with support of the silver and metalized by carbon deposited in two orientations (20°–30°). During the SEM photography, qualitative microanalysis was done to confirm the presence of different phases in the system.

2.4. Zeta potential

The fine earth fractions of materials used in the experiments were ground in an agate mortar, and then re-dispersed in water and various solutions. For the electrophoresis experiment, we used the supernatant of the suspension obtained after sedimentation, resulting a volume fraction of 0.5 g/l. Electrokinetic properties of the studied systems were analyzed with a Malver-ZetaSizer 3000 HS, based on electrophoretic mobility measurements. For each treatment, the powder material was conditioned for 24 h in 1 l of solution at the required concentrations, for different electrolytes.

2.5. Surface free energy

To estimate the surface free energy of the samples, we used a method with measurement of advancing contact angles of three probe liquids (diiodomethane, water, and formamide) of known surface-tension components onto dry soil pellets. For this purpose, a ramé-hart Instrument Co. (New Jersey, USA) NRL CA goniometer was used. Images of drops placed on the surface were captured by a video camera adapted to the goniometer, immediately after their deposition with a Gilmont (USA) micrometer syringe. Prior to contact angle measurements, the soil was dried at 343,15 °C and kept in a desiccator. Only stable drops were used to compute surface free energy components of the solids. The contact angles of water, formamide, and diiodomethane were measured on pellets of these materials. The pellets made by compressing dry powder under 5.5 × 104 kg/cm^2 for 10 min. Only pellets having a smooth, specular surface (at the optical microscope level) were selected. The contact angle was recorded immediately after depositing the drop.

2.6. Introduction to interfacial theories

The process of adhesion between particles of colloidal size dispersed in a water medium is determined by the balance of forces between various phases that coexist in the system, namely, hydrodynamic, diffusive-type, and interfacial forces. At short distances, The interfacial forces are the responsible of interactions between particles. Three kinds of interfacial interactions should be considered, electrostatic (EL), Lifshitz–van der Waals (LW), and acid-base (AB).

2.6.1. Electrical characterization

For electrical characterization, zeta potential ζ was calculated based on the Smoluchowski (Smoluchowski, 1921) relationship:

$$\xi_{EP} = \frac{V\mu}{\varepsilon E_x}, \tag{1}$$

where ξ_{EP} is the electrophoretic ζ, V is electrophoretic velocity, and μ and ε are the viscosity and permittivity of the medium, respectively. E_x is the axial electric field. The Smoluchowski equation is a simplified approach; the electrostatic driving force is opposed by the frictional force and other effects are neglected. That equation is valid for solid particles with large dimensionless inverse Debye length (Wang and Revil, 2010). The equation gives good results only for large colloidal particles and high ionic strengths when ζ is not too high (<120 mV). In our experiments the Smoluchowski approximation was acceptable; specifically, particle size of a micrometer and ionic strength 1 mM, and $\zeta \ll 120$ mV.

2.6.2. Surface free-energy determination

Detailed descriptions of surface free energy formulation have been given in numerous papers (Van Oss, 1994). Thus, the total surface free energy of a solid or liquid is described as the sum of the dispersive Lifshitz - van der Waals component $\gamma^{LW}{}_S$ and polar acid-base interaction $\gamma^{AB}{}_S$, which is in many cases due to hydrogen bonding. In general, the polar γ^{AB} interaction is caused by electron-donor (γ^-) and electron-acceptor (γ^+) contributions. The relationship between contact angle θ and the LW and (Lewis) AB components of the surface free energy of the solid (subscript 1) and surface tension of the liquid (subscript 3) can be written as

$$2\sqrt{\gamma_1^{LW}\gamma_{Li}^{LW}} + 2\sqrt{\gamma_1^{+}\gamma_{Li}^{-}} + 2\sqrt{\gamma_1^{-}\gamma_{Li}^{+}} = \gamma_{Li}(1 + \cos\theta), \tag{2}$$

where γ_{Li} is the surface tension of liquid i forming contact angle θ on the solid, and $\gamma^{LW}{}_{Li}$, $\gamma^{+}{}_{Li}$, and $\gamma^{-}{}_{Li}$ are the surface tension components of the liquid. Thus, by measuring the contact angles of the aforementioned three liquids, a system of three equations of type (2) can be resolved to attain the three unknown variables γ_1^{LW}, γ_1^{+} and γ_1^{-}.

2.7. Interfacial interactions between two similar particles in aqueous media

For colloidal-sized particles, transport, deposition and mechanical stability of the final deposit are strongly influenced by surface interactions between particles dispersed in water. According to extended Derjaguin–Landau–Verwey–Overbeek (DLVO) theory (Van Oss, 1994), three types of interfacial interactions should be considered: Lifshitz-van der Waals (LW), electrostatic (EL), and acid–base (AB). The three contributions depend on the nature of the interfaces involved (i.e., the zeta potential and surface free energy components). For particles

(phase 1) of the same material dispersed in water (phase 3), total interaction energy between the particles is given by

$$\Delta G_{131}^{TOT} = \Delta G_{131}^{EL} + \Delta G_{131}^{LW} + \Delta G_{131}^{AB}, \quad (3)$$

where subscript 131 refers to the phases involved. In our case, it refers to particle - liquid medium - particle in the aggregation process. The three contributing interactions depend on the nature of the interfaces involved and on the distance H between surfaces. Under the constant potential, double-layer model for moderate potentials, the electrostatic interactions can be obtained from Duran et al. (1998):

$$\Delta G_{131}^{EL} = 2\pi\varepsilon a\xi^2 \ \ln\left(1 + e^{-\kappa H}\right). \quad (4)$$

where ζ is the zeta potential, a is particle radius ε the dielectric constant of the liquid, and κ is the Debye screening length (double-layer thickness).

Corresponding expressions for LW interaction are

$$\Delta G_{131}^{LW} = -\frac{A_{131}}{6}\left(\frac{2a^2}{H(4a+H)} + \frac{2a^2}{(2a+H)^2} + \ln\frac{H(4a+H)}{(2a+H)^2}\right), \quad (5)$$

where A_{131} is the Hamaker constant for each system, which can be estimated by surface tension determination of the materials involved. We used the thermodynamic treatment proposed by Van Oss (1994) for a full account of the theory. According to those authors, the surface free energy (or surface tension) γ_i of a condensed phase consists of two additive contributions, dispersive LW and polar AB, which in turn depend on two parameters accounting for the γ^- and γ^+ characters of the materials ($\gamma i = 2(\gamma_i + \gamma_i -)^{1/2}$). If γ_i^{LW} is known for all phases involved, the Hamaker constant can be obtained as

$$A_{131} = 12\pi H_0^2 \Delta G_{131,H_0}^{LW} \quad (6)$$

$$\Delta G_{131,H_0}^{LW} = -2\left(\sqrt{\gamma_1^{LW}} - \sqrt{\gamma_3^{LW}}\right)^2, \quad (7)$$

where H_0 is estimated at 1.58 ± 0.08 Å (Van Oss et al., 1988). Similarly, the calculation of H-dependence of ΔG_{AB}^{131} requires knowledge of γ^+ and γ^- for the two phases.

$$\Delta G_{131}^{AB} = 2\pi a\lambda \Delta G_{131,H_0}^{AB} e^{\left(\frac{H_0 - H}{\lambda}\right)}, \quad (8)$$

where λ is the correlation length of water molecules, approximately λ = 1 nm for hydrophilic surfaces, and ΔG_{131} depends on the acid-base parameters of the free energy of phases 1 and 3 (Van Oss, 1994; Ontiveros et al., 1996).

According to van Oss, the quantity $\Delta G^{AB}{}_{131}$, H_0 is:

$$\Delta G_{131,H_0}^{AB} = 4\left(\sqrt{\gamma_1^+\gamma_1^-} + \sqrt{\gamma_3^+\gamma_3^-} - \sqrt{\gamma_1^+\gamma_3^-} - \sqrt{\gamma_3^+\gamma_1^-}\right) \quad (9)$$

3. Results and discussion

3.1. Chemical and mineralogy analyses and SEM photography

Chemical analyses of the sample indicate a typical content of silica in the rocks, if we represent the content of $Na_2O + K_2O$ with regard to SiO_2 (Table 1(a-b) and Fig. 2). In the Fig. 3 we can see the content of K_2O with regard to SiO_2, K diagram.

The chemical composition of Almagre shows that the SiO_2 content (58.6%). Accoding to the TAS Diagram (e.g. Streckeisen et al., 2002, p.526) the rock composition was intermediate with high in alkalis content ($NaO + K_2O$). This indicates the presence of heavy elements such as Zr, Sr, and Ti. Light elements are also present as phosphates, sulfates and chlorides. However, the most striking finding is the content of organic matter (7.3%) as compared to virgin eruptive materials, indicating that the substance has been subjected to the action of edaphological processes.

Table 1
X-ray fluorescence (XRF) analysis for Almagre.

(a)	
Minerals	%
Q	5,13
Cor	1,49
Ort	27,65
Ab	53,16
An	5,91
Hy	2,23
Hem	3,9
Ilm	0,09
Ap	0,23
Py	0,34
%An en Pl	10
ITT	91,85

(b)	
Oxides	%
LOI	7,3
Na_2O	5,8
MgO	0,83
Al_2O_3	17,6
SiO_2	58,6
P_2O_5	0,091
SO_3	0,17
Cl	0,21
K_2O	4,32
CaO	1,22
TiO_2	0,784
MnO	0,15
Fe_2O_3	3,6
SrO	0,023
ZrO_2	0,0919
Total	100,78

It is evident that the rock is called trachyandesite, specifically banakite. It is a rock of explosive type associated with an index of volcanic explosivity III/IV. We also found a high content of Fe.

However, Table 1-b shows the mineralogical theoretical composition calculated from the Norm CIPW (Cross, Iddings, Pirsson and Washington) (Verma and Navarro de León, 1993), indicating that near 60% of the rock is plagioclase, 27% pyroxene, 5% quartz, and the incidental minerals cordierite and apatite.

SEM (Fig. 4) revealed the components of the studied sample.

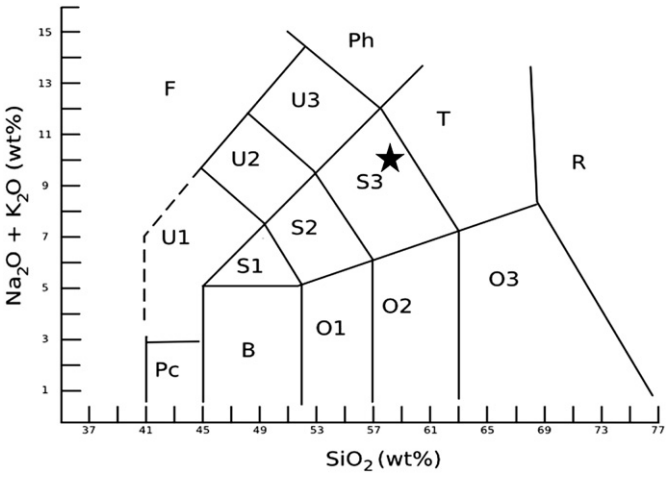

Fig. 2. Classification of studied of Alamgre according to total alkaline vs. SiO_2 (TAS) diagram.

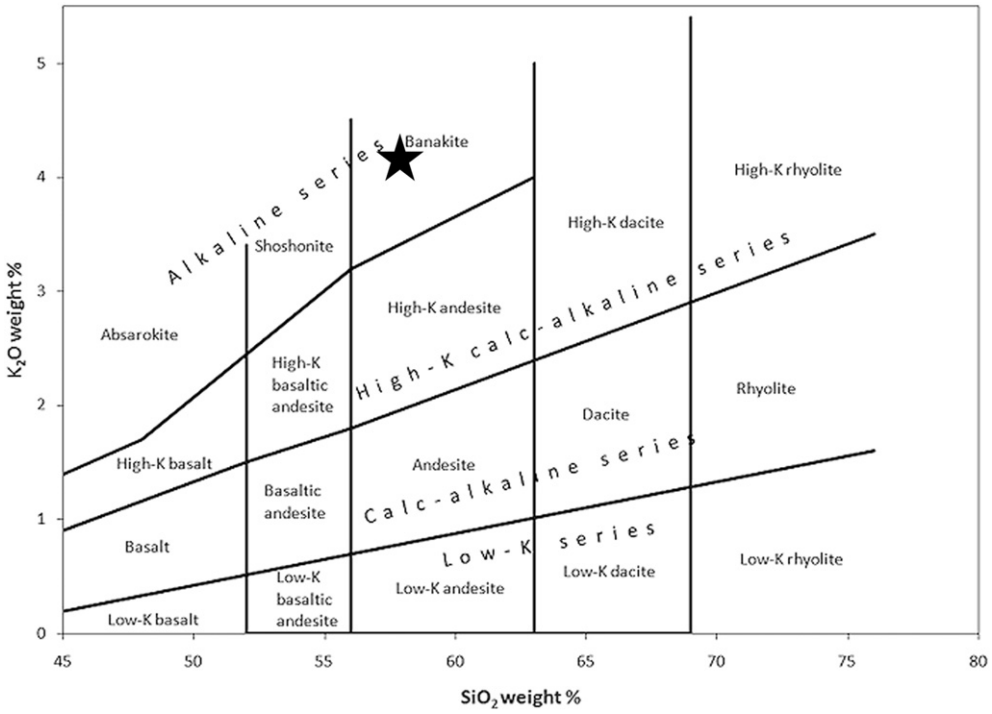

Fig. 3. Classification of studied of Alamgre, according to K_2O vs. SiO_2 diagram for rock series %K diagram.

It is evident that the rock is constituted by various components: volcanic glasses of different forms (plane D; sphere E, chaotic B and F) and components with a soil structure (A, C, and E) with domains and micro-domains.

In the photography we observed that the components are distributed in random form within the rock. The various forms and sizes of volcanic crystal (B, D and F) and components with the structure of domains and micro-domains (A, C and E) indicate a chaotic origin and rapid emplacement.

3.2. Electrical characterization of Almagre: potential zeta

Figs. 5–7 show values of ζ as a function of pH for different electrolytes (monovalent, divalent and trivalent) and concentrations.

In general, ζ values are negative for monovalent and divalent electrolytes, Almagre is considered to be ~59% SiO_2 (Table 1). The surface is negative because of the existence of SiO^- groups. The strong decrease at acidity pH (between 2 and 4) is likely attributable to the progressive adsorption of Cl^- ion groups at the interface. At higher pH, the behavior

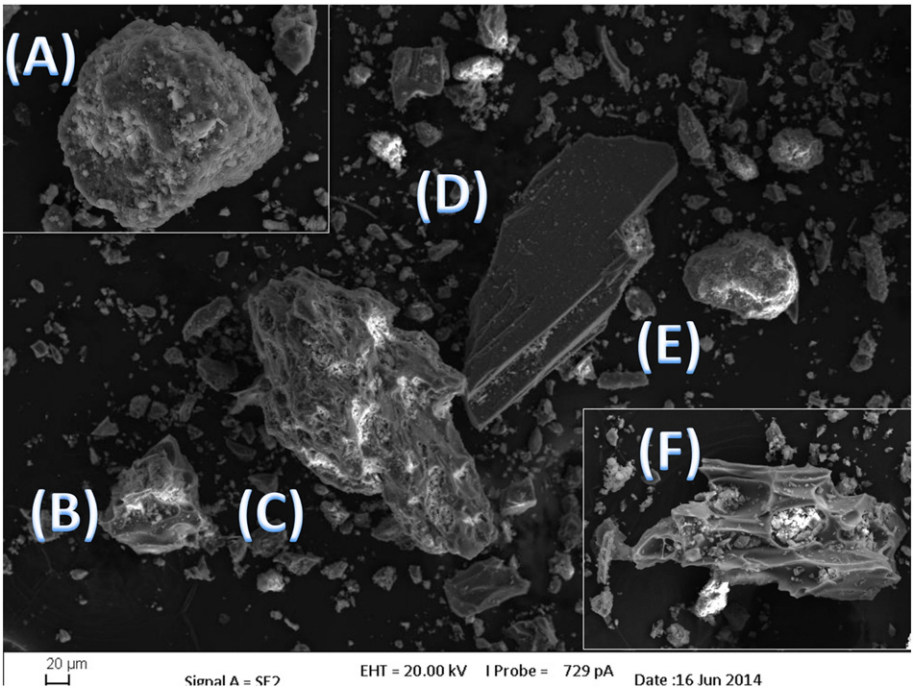

Fig. 4. SEM images of Almagre material.

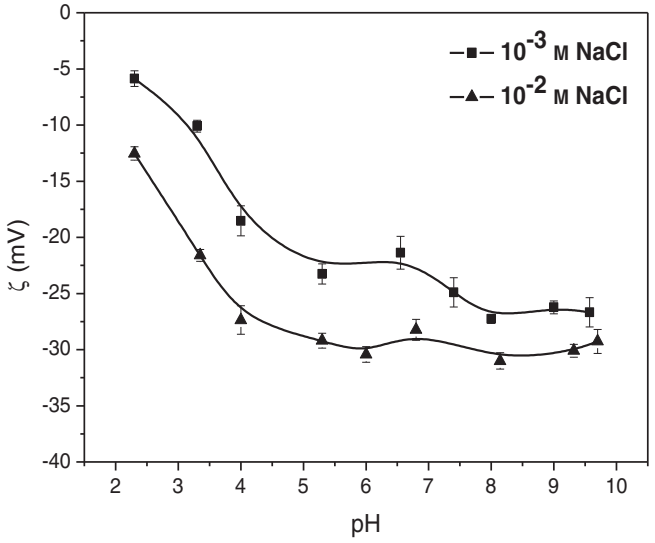

Fig. 5. Zeta potential (ζ) of Almagre as function of pH value for 1 and 10 mM concentrations of NaCl.

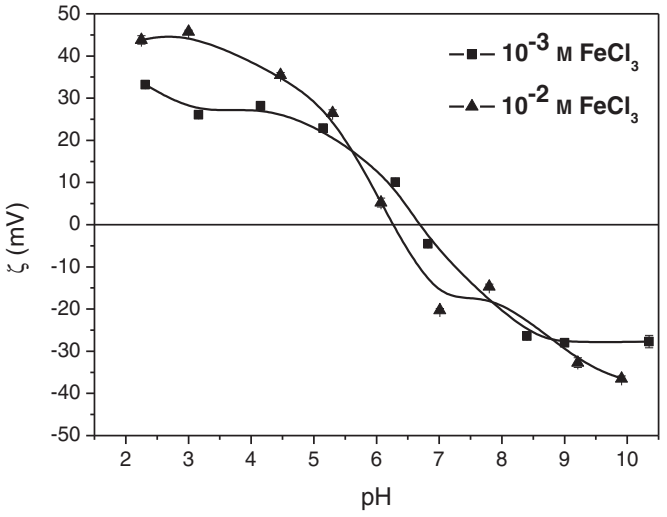

Fig. 7. Zeta potential (ζ) of Almagre as function of pH value for 1 and 10 mM concentrations of $FeCl_3$.

can be ascribed to equilibrium between the absorption of cations at the interface and progressive adsorption of hydroxyl groups.

The mean ζ of soil in the presence of Na^+ and in various pH conditions is shown in Fig. 5. Mean ζs were negative in pH range 2–10. Mean ζ magnitudes were linearly proportional to pH in the solution for pH 2–6, but had relatively constant values at higher pH. This decrease (between 5 and 30 mV in absolute value) can be attributed to a progressive adsorption of Cl^- ions onto soil particles. Fig. 5 also shows ζ behavior for different ionic strengths of the medium. The results show that ζ for an electrolyte concentration of 0.01 M was higher than that for 0.001 M NaCl in solution. This is anomalous behavior is due probably from increased ionic strength leading to particle coagulation, which produces particles of larger radius. This in turn produces larger values of κa and therefore ζ (Plaza et al., 2015). This behavior may be also associated with an excess of electrical charge at the interface, which controls surface conductivity. In fact, the interpretation of electrophoretic mobilities of particles is complex because of such excess charge (Tejada et al., 2009). In any case, in general we can say that an increase of pH implies an increase of the surface charge, and an increase of the repulsion between particles, therefore, a decrease of the coh In

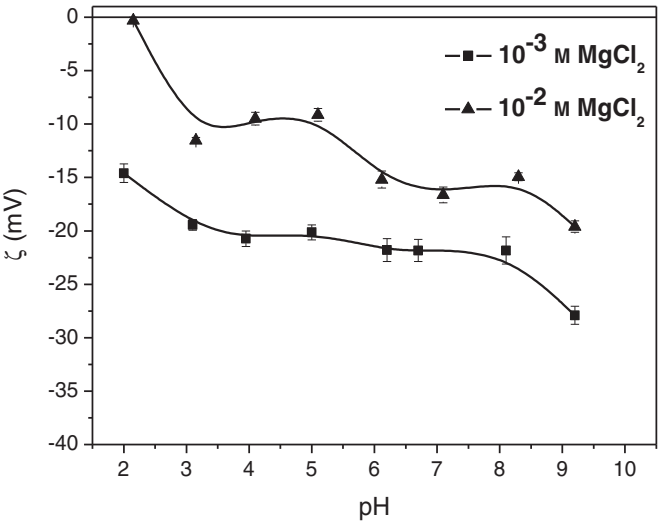

Fig. 6. Zeta potential (ζ) of Almagre as function of pH value for 1 and 10 mM concentrations of $CaCl_2$.

any case, in general we can say that an increase of pH implies an increase of the surface charge, and an increase of the repulsion between particles, therefore, a decrease of the cohesionesion.

Fig. 6 depicts the ζ behavior of soil in the presence of a divalent electrolyte Mg^{+2}. In this case, ζ was also negative for all pH, but its obtained values (between 0 and 15 mV in absolute value) were smaller than for the monovalent electrolytes. We see that the dependence on pH in this case is weaker, as expect from a divalent electrolyte. This behavior was explained by Lagaly (2006). This process may be attributable to the behavior of the gels of alumina and allophane present in the majority of Andisols (FAO, 2006). Regarding the effect of ionic strength, we observed a decrease in ζ with increasing electrolyte concentrations, owing to compression of the double electrical layer.

In the case of trivalent electrolyte Fe^{+3} (Fig. 7), ζ had a double electrical nature, positive in acid medium and negative at basic pH. The zero-charge point in the case of the iron reached pH 6 to 7. Fe^{3+} cations were absorbed onto particles, probably because of acid pH values. The ζ of the system decreased to +45 to 0 mV, ascribed to progressive adsorption of Cl^- and hydroxyl groups with increasing pH. For the largest values of pH, the negative ζ may be attributable to the formation of coordination compounds, indicating that the iron is adsorbed in the form of $Fe(OH)^{2+}$ and $Fe(OH)^+$.

3.3. Surface free energy

Table 2 lists components of surface free energy obtained from the sample, in natural conditions and after treatments with electrolytes of Na, Mg and Fe.

The Almagre in bare conditions has a dispersive component γ^{LW} with a value of 47 mJ/m^2, Analogous results have been obtained for samples rich in silicon oxide by other authors (A. Ontiveros-Ortega et al., 2014–2016) and (Ramos-Tejada et al., 2003). The treatment with the iron electrolyte did not modify the initial characteristics of

Table 2
Values of LW component γ^{LW}, electron-acceptor γ^- and electron-donor γ^+ parameters of AB component of surface free energy for Almagre.

	γ^{LW}(mJ/m²)	γ^-(mJ/m²)	γ^+(mJ/m²)	γ^{TOT}(mJ/m²)
Almagre	46,941	36,071	0,57,962	56,086
Almagre + NaCl	40,602	18,113	2,8704	55,022
Almagre + MgCL	44,222	20,885	1,2612	54,487
Almagre + FeCl	45,028	38,928	0,6561	55,135

the sample under natural conditions, likely because of the high iron content in the Almagre; see in Table 2. We see that the γ^{LW} component decreases as we move down the valence of the cation present, e.g., 6 units for the treatment with Na^+ and 3 with Mg^{2+}.

The results for the polar components show that in bare conditions, the sample had a monopole character ($\gamma^+ = 0$ and $\gamma^- \neq 0$), and was electron-donor in nature. The treatments with electrolytes Na and Mg (both very common ions in the sea breeze) reduced γ^- from 36 to 18 and 20 mJ/m^2, respectively, causing the sample go from hydrophilic to hydrophobic ($\gamma^- < 28$ mJ/m^2) according to Van Oss et al. (1988). This indicates a less wettable sample (for an equal pore size).

The result for the γ^+ parameter shows an increase from 0.6561 (Fe^{3+}) to 1.26 mJ/m^2 (Mg^{2+})) and 2.87 mJ/m^2 (Na^+). The effect of electrolytes conferred a slight bipolar character, and there was γ^+ decrease with increasing valence of the absorbed cation.

3.4. Energy of interaction

Qualitative explanation of the cohesion of soil has been given in terms of the total energy of interaction between the particles themselves, computed from the extended DLVO theory, including both the energy of interaction of the double layers (DG_{El}) and the energy of interaction of the particles themselves, owing to van der Waals (DG_{LW}) and polar or acide-base (DG_{AB}) interaction forces. In Figs. 8–10, we can see typical plots of the total potential energy DG_{TOT} of interaction between the soil particles, as a function of their separation H. When the surface potentials of the two interacting surfaces are large and have the same sign, then DG_{EL} is positive. Physically, this means that the particles must pass over a potential barrier before adhesion can take place. When the surface potentials are very small or of opposite sign, there is no barrier and rapid adhesion may take place. The rate of adhesion will depend to some extent on the magnitude of DG_{TOT}; this dependence has yet to be expressed quantitatively. Having obtained the zeta potentials and surface free energies of soil particles, the potential energies of interaction between surfaces were calculated. To interpret these cohesion variations, we compared the total energy of interaction between the particles in the different experimental conditions.

Figs. 8–10 show curves of interaction energy, calculated from Table 3 and Eqs. 4,5 and 8 as a function of distance (H) between particles.

Fig. 8 shows the obtained energy interactions between particles for the sample with Na^+ at different ionic strengths. These must overcome a barrier of potential that becomes greater with increasing proximity between particles, with maxima at very short distances ($H \leq 5$ nm). These barriers increase with pH. A qualitative description suggests that for pH = 3, the barrier of potential has values on the order of

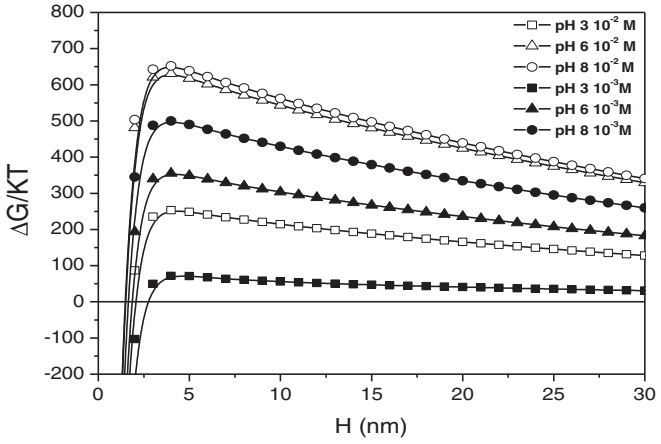

Fig. 8. Total energy of interaction (in kT) between particles as the function of the distance between surfaces, H, for different pH values and ionic strength when the electrolyte present in solutions was NaCl.

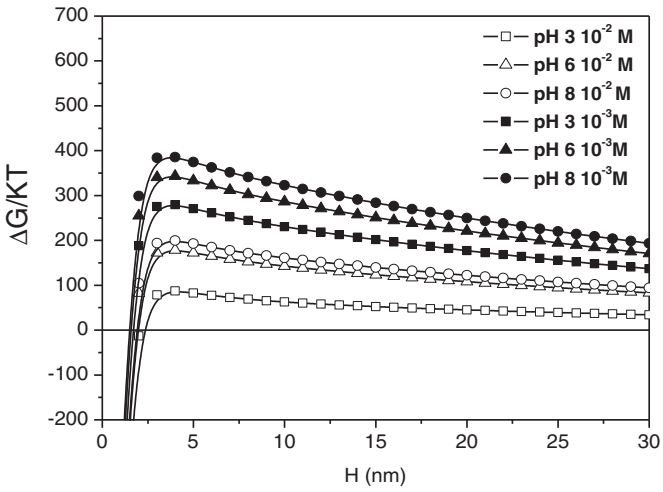

Fig. 9. Total energy of interaction (in kT) between particles as the function of the distance between surfaces, H, for different pH values and ionic strength when the electrolyte present in solutions was $CaCl_2$.

50 kT. This is an approximation for the particles of Almagre, indicating a cohesive behavior. At more basic pH, the barriers strengthen, resulting in a less cohesive deposit. Because of the large ζ values shown in Fig. 5, for low ion concentrations of Na, potential barriers at lower ionic strengths are stronger than those at greater strengths.

Fig. 9 shows curves obtained for Mg at different ionic strengths (0.001 and 0.01 M) and pH values (3, 6, and 8). In all cases, barriers of potential are >75 kT, suggesting that the particles cannot approach each other and so the soil will have a low degree of compaction. For pH behavior observed in Fig. 9, the results show that the deposit is weakly cohesive for all pH. It is also evident that repulsion between particles is weakest for the highest concentrations of cations in the solution.

Fig. 10 shows curves of energy obtained for the treatment with iron. The anomalous behavior of the energy of interaction when iron is observed. We can observed that in acid values (pH = 3), the particles showed the maximum repulsion of all studied conditions. This confirms that an acid contribution to deposits of Almagre drastically reduces cohesion between the particles, which would cause strong instability. In contrast, for pH = 6, the Almagre substrate was the most stable, with smaller values of potential barrier.

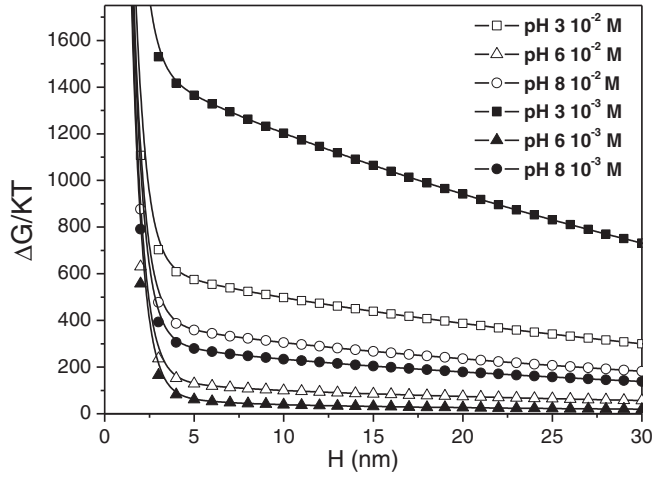

Fig. 10. Total energy of interaction (in kT) between particles as the function of the distance between surfaces, H, for different pH values and ionic strength when the electrolyte present in solutions was $FeCl_3$.

Table 3
Parameters used to calculate the potential energy of interaction between particles.

	Zeta potencial (mV) without electrolytes			SFE			
	pH 3	pH 6	pH 8	LW	+	–	Total
Sample	−6.05	−10,48	−13,88	46,941	0,5796	36,071	56,086

	pZ 0.001 M			pZ 0.01 M			LW	+	–	Total
NaCl	−8.75	−22.17	−26.5	−18.5	−29.89	−30.4	40,602	2,8704	18,113	55,022
$MgCl_2$	−19.59	−21.36	−22.76	−9.06	−14.7	−15.7	44,222	1,2612	20,885	54,487
$FeCl_3$	44.6	6.4	−19.15	28.44	11.96	−22.05	45,028	0,6561	38,928	55,135

4. Summary and conclusions

The sea breeze over the hillsides of the volcanic islands increases the contents of sodium and magnesium of Almagre. This alters superficial properties (surface free energy and ζ) of the material composing the substratum. This alteration affects the water retention and cohesion of the material constituting the deposit. We analyzed the effects that produce sodium, magnesium, and iron through the surface free energy and superficial charge of the deposit.

We studied the effects that produce the sodium and magnesium absorbed by Almagre. The results of the surface free energy analysis show an increase in hydrophobicity of the material, which induces a weak capacity of water retention and thereby increased surface runoff. However, analysis of the energy of total interaction in the sample under very acidic (pH = 3) conditions revealed that the electrolytes of sodium and magnesium induce strong cohesion relative to a basic pH. At basic pH (remember natural pH for Almagre is 8), there is clear repulsion between the particles.

We also studied the effect of the presence of iron on our material. The results show that when there is dissolved iron, the repulsion between particles is greater than that obtained with the other electrolytes. This emphasizes that Almagre is a substratum very rich in iron that can contributed to dissolution under saturated conditions. This suggests that a saturated Almagre continues to be an ideal layer for sliding.

Acknowledgements

We gratefully acknowledge the support of institutions involved. This work was partially funded by Projects, "KNOWLEDGE EXTRACTION OF THE STATE OF ACTIVE VOLCANOES AND ITS APPLICATION TO THE MODELLING OF ERUPTION FORECAST BY ADVANCED SEISMIC SIGNAL ANALYSIS (KNOWAVES) (TEC2015-68752-R)". We also thank National Geographical Institute of the Spanish Ministry and the two anonymous reviewers whose constructive comments have considerably improved the quality of this work.

References

Ancochea, E., Fuster, J., Ibarrola, E., Cendrero, A., Coello, J., Hernan, F., Jamond, C., 1990. Volcanic evolution of the island of Tenerife (Canary Islands) in the light of new K-Ar data. J. Volcanol. Geotherm. Res. 44 (3–4), 231–249.

Ancochea, E., Huertas, M.J., Cantagrel, J.M., Coello, J., Fúster, J.M., Arnaud, N., Ibarrola, E., 1999. Evolution of the Cañadas edifice and its implications for the origin of the Cañadas Caldera (Tenerife, Canary Islands). J. Volcanol. Geotherm. Res. 88 (3), 177–199.

Bailey, C., Fodor-Csorba, K., Gleeson, J.T., Sprunt, S.N., Jákli, A., 2009. Rheological properties of bent-core liquid crystals. Soft Matter 5 (19), 3618–3622.

BASU, S.R., DE, S.K., 2003. Causes and consequences of landslides in the Darjiling-Sikkim Himalayas, India. Geogr. Pol. 76 (2), 37–52.

Baumgarten, W., Neugebauer, T., Fuchs, E., Horn, R., 2012. Structural stability of marshland soils of the riparian zone of the tidal Elbe River. Soil Tillage Res. 125, 80–88.

Baumgarten, W., Dörner, J., Horn, R., 2013. Microstructural development in volcanic ash soils from South Chile. Soil Tillage Res. 129, 48–60.

Blight, G.E., 1997. Mechanics of Residual Soils. Balkema, Rotterdam.

Bommer, J.J., 2002. Deterministic vs. probabilistic seismic hazard assessment: an exaggerated and obstructive dichotomy. Journal of Earthquake Engineering 6, 43–73 spec01.

Broothaerts, N., Kissi, E., Poesen, J., Van Rompaey, A., Getahun, K., Van Ranst, E., Diels, J., 2012. Spatial patterns, causes and consequences of landslides in the Gilgel Gibe catchment, SW Ethiopia. Catena 97, 127–136.

Carracedo, J.C., Badiola, E.R., Guillou, H., Paterne, M., Scaillet, S., Torrado, F.P., Hansen, A., 2007. Eruptive and structural history of Teide volcano and rift zones of Tenerife, Canary Islands. Geol. Soc. Am. Bull. 119 (9–10), 1027–1051.

Carracedo, J.C., Fernandez-Turiel, J.L., Gimeno, D., Guillou, H., Klügel, A., Krastel, S., Troll, V.R., 2011. Comment on "the distribution of basaltic volcanism on Tenerife, Canary Islands: implications on the origin and dynamics of the rift systems" by A. Geyer and J. Martí. Tectonophysics 483 (2010) 310–326. Tectonophysics 503 (3), 239–241.

Churakov, S.V., Gimmi, T., 2011. Up-scaling of molecular diffusion coefficients in clays: a two-step approach. J. Phys. Chem. C 115 (14), 6703–6714.

Cockell, C.S., 2010. Geomicrobiology beyond earth: microbe–mineral interactions in space exploration and settlement. Trends Microbiol. 18 (7), 308–314.

Crozier, M.J., Glade, T., 2005. Landslide hazard and risk: issues, concepts and approach. Landslide Hazard and Risk 1–40.

Duran, J.D.G., Ontiveros, A., Delgado, A.V., Gonzalez-Caballero, F., 1998. Kinetics and interfacial interactions in the adhesion of colloidal calcium carbonate to glass in a packed-bed. Appl. Surf. Sci. 134 (1), 125–138.

FAO, 2006. World Base Reference for Soil Resources. Report on World Soil Resources. FAO, Rome, Italy.

Holtz, R.D., Kovacs, W.D., 1981. An Introduction to Geotechnical Engineering (No. Monograph).

Hürlimann, M., Martı´, J., Ledesma, A., 2004. Morphological and geological aspects related to large slope failures on oceanic islands. The huge La Orotava landslides on Tenerife, Canary Islands. Geomorphology 62, 143–158 (Iuss, I. (2006)).

Kadar, E., Fisher, A., Stolpe, B., Calabrese, S., Lead, J., Valsami-Jones, E., Shi, Z., 2014. Colloidal stability of nanoparticles derived from simulated cloud-processed mineral dusts. Sci. Total Environ. 466, 864–870.

Katsuta, N., Shimizu, I., Helmstaedt, H., Takano, M., Kawakami, S., Kumazawa, M., 2012. Major element distribution in Archean banded iron formation (BIF): influence of metamorphic differentiation. J. Metamorph. Geol. 30 (5):457–472. https://doi.org/10.1111/j.1525-1314.2012.00975.

Lagaly, G., 2006. Colloid clay science. In: Bergaya, F., Theng, B.K.G., Lagaly, G. (Eds.), Handbook of Clay Science. Elsevier, Amsterdam, pp. 247–260.

Longpré, M.A., Troll, V.R., Walter, T.R., Hansteen, T.H., 2009. Volcanic and geochemical evolution of the Teno massif, Tenerife, Canary Islands: some repercussions of giant landslides on ocean island magmatism. Geochem. Geophys. Geosyst. 10 (12).

Martí, J.H., 1997. Vertical and lateral collapses on Tenerife (Canary Islands) and other volcanic ocean islands. Geology 25 (10), 879–882.

Masson, D.G., Watts, A.B., Gee, M.J.R., Urgeles, R., Mitchell, N.C., Le Bas, T.P., Canals, M., 2002. Slope failures on the flanks of the western Canary Islands. Earth Sci. Rev. 57 (1), 1–35.

Ontiveros, A., Duran, J.D.G., Gonzalez-Caballaro, F., Chibowski, E., 1996. Adhesion of colloidal ZnS on silicon. Effects of ionic strength and radio frequency electric field. J. Adhes. Sci. Technol. 10, pp. 999–1019.

Ontiveros-Ortega, A., Vidal, F., Gimenez, E., Ibáñez, J.M., 2014. Effect of heavy metals on the surface free energy and zeta potential of volcanic glass: implications on the adhesion and growth of microorganisms. J. Mater. Sci. 49 (9), 3550–3559.

Ontiveros-Ortega, A., Moleon, J.A., Plaza, I., Guillén, C., 2016. Effect of interfacial properties on mechanical stability of ash deposit. J. Rock Mech. Geotech. Eng. 8 (2), 187–197.

Perkins, Sid, 2009. The iron record of Earth's oxygen. Science News 175, 24 1943-0930.

Plaza, I., Ontiveros-Ortega, A., Calero, J., Aranda, V., 2015. Implication of zeta potential and surface free energy in the description of agricultural soil quality: effect of different cations and humic acids on degraded soils. Soil Tillage Res. 146, 148–158.

Ramos-Tejada, M.M., Ontiveros, A., Viota, J.L., Durán, J.D.G., 2003. Interfacial and rheological properties of humic acid/hematite suspensions. J. Colloid Interface Sci. 268 (1), 85–95.

Rošic, R., Pelipenko, J., Kocbek, P., Baumgartner, S., Bešter-Rogač, M., Kristl, J., 2012. The role of rheology of polymer solutions in predicting nanofiber formation by electrospinning. Eur. Polym. J. 48 (8), 1374–1384.

Smoluchowski, M.V., 1921. Handbook of Electricity and Magnetism. Barth, Leipzig. 366.

Soto, E.A., Coronel, M.J.H., Cantagrel, J.M., Coello, J., Casas, J.M.F., Arnaud, N., Ibarrola, E., 1999. Evolution of the Cañadas Edifice and its Implications for the Origin of the Cañadas Caldera (Tenerife, Canary Islands).

Streckeisen, A., Zanettin, B., Le Bas, M.J., Bonin, B., Bateman, P., Bellieni, G., Dudek, A., Efremova, S., Keller, J., Lamere, J., Sabine, P.A., Schmid, R., Sorensen, H., Woolley, A.R., 2002. Igneous Rocks: A Classification and Glossary of Terms, Recommendations

of the International Union of Geological Sciences. Subcommission of the Systematics of Igneous Rocks. Cambridge University Press.
Tejada, M., Hernandez, M.T., Garcia, C., 2009. Soil restoration using composted plant residues: effects on soil properties. Soil Tillage Res. 102 (1), 109–117.
Van Oss, C. J., Chaudhury, M. K., & Good, R. J. (1988). Interfacial Lifshitz-van der Waals and polar interactions in macroscopic systems. Chem. Rev., 88(6), 927–941.
Van Oss, C.J., 1994. Polar or Lewis acid-base interactions. Interfacial forces in aqueous. Media 18–46.
Verma, S.P., Navarro de León, I., 1993. Norma CIPW–Nuevo programa de cómputo. México, DF, Instituto de Geofísica, 3er. Congreso Nacional de Geoquímica, Memorias, pp. 117–119.
Wang, M., Revil, A., 2010. Electrochemical charge of silica surfaces at high ionic strength in narrow channels. J. Colloid Interface Sci. 343 (1), 381–386.
Zhou, G., Esaki, T., Mitani, Y., Xie, M., Mori, J., 2003. Spatial probabilistic modeling of slope failure using an integrated GIS Monte Carlo simulation approach. Eng. Geol. 68 (3), 373–386.